Removal of HCl from Gases Using Modified Calcined Mg-Al-CO_3 Hydrotalcite: Performance, Mechanism, and Adsorption Kinetics

Songshan Cao[1, 2], Jun Cao[3], Hualun Zhu[2], Yaji Huang[1], Baosheng Jin[1]*, Massimiliano Materazzi[2]*

1 Key Laboratory of Energy Thermal Conversion and Control of Ministry of Education, School of Energy and Environment, Southeast University, Nanjing, 210096, China.

2 Department of Chemical Engineering, University College London, London WC1E 7JE, United Kingdom.

3 National Engineering Research Center of Water Resources Efficient Utilization and Engineering Safety, Hohai University, Nanjing 211111, China.

**Corresponding author. Baosheng Jin and Massimiliano Materazzi*

Email: bsjin@seu.edu.cn (Baosheng Jin)

massimiliano.materazzi.09@ucl.ac.uk (Massimiliano Materazzi)

Abstract: To achieve carbon neutrality, it is essential to remove HCl resulting from the extensive use of alternative fuel feedstock in thermochemical plants. In this work, the HCl removal performance of modified calcined Mg-Al hydrotalcite (Mg-Al-CO_3) on gaseous stream was investigated. The layered structure of Mg-Al-CO_3 intercalated with CO_3^{2-} was successfully prepared using the coprecipitation method with a molar ratio of Mg/Al equal to 3.1. The optimal performance of Mg-Al-CO_3 for HCl removal was observed at 300 °C, and the breakthrough chlorine capacity was 102.7 mg g^{-1}. Among calcined Mg-Al samples, only Mg-Al-400 exhibited better HCl removal performance than Mg-Al-CO_3. The specific surface area of Mg-Al-400 was 183.73 m^2 g^{-1}, which was 2.8 times greater than that of Mg-Al-CO_3. The average HCl removal rate was 90.11% within the first 120 min, which was 1.12 times higher than that of Mg-Al-CO_3. Moreover, the breakthrough chlorine capacity of Mg-Al-400 was increased by 16.9%, reaching 120.1 mg g^{-1}. Two reaction paths were identified for Mg-Al-400, first Mg^{2+} reacts with Cl^- to generate $MgCl_2$, and then Cl^- acted as a new interlayer anion of hydrotalcite. According to the results of adsorption kinetics, the pseudo-second-order and the Bangham model were found to fit well with the HCl removal process of Mg-Al-400.

Keywords: Waste incineration; Gas cleaning; Calcined Mg-Al, HCl removal, Adsorption kinetic

1 Introduction

Recently, carbon zero and carbon neutrality have become hot topics due to the serious problem

of greenhouse gas emissions[1, 2]. The increase in global temperature caused by greenhouse gases has seriously affected human survival[3]. To address this issue, the countries around the world have formulated policies and set targets to reduce carbon emissions and achieve carbon neutrality across all sectors. The combustion of fossil fuels is one of the primary sources of CO_2 emission as part of industrial processes[4]. One effective way to reduce carbon emissions is to choose suitable fuels to replace traditional ones. Up to now, combustible solid waste, which had potential calorific value, has been widely recognized as alternative fuel, such as biomass, domestic garbage, industrial waste, and so on[5-7]. Owing to the rapid development of industry and population growth, large amounts of solid waste are produced, leading to a series of social and environmental problems[8, 9]. The urgent need to treat waste in a harmless way has become increasingly clear. The use of combustible solid waste as fuel not only meets the demand with reducing carbon dioxide emission, but also enables resource recovering and recycling simultaneously[10, 11]. These alternative fuels have been applied in various fields, including power plants, cement plants, and more[12-14].

However, the promotion of alternative feedstock has also led to new problems. In the process of thermal conversion, the emission of new contaminants had become a problematic issue[15]. The gaseous HCl, as one of classic gaseous pollutants, has increased in exhaust gas[16, 17]. This increase is attributed to the higher content of chlorine in waste plastics, and other biomass streams [18]. The increased HCl brought about a series of negative issues. For instance, the presence of large amounts of HCl in industrial equipment system can lead to both high and low temperature corrosion issues. It can also promote and combine with alkali metals in biomass to generate alkali metal salts, causing corrosion, fouling and slagging of downstream devices, ultimately reduce the lifespan of devices and increases maintenance costs and operates risks[19]. In addition to damaging equipment, HCl is one of the most significant contributors to acid rain formation. If it is discharged into the atmosphere, it can not only harm the environment but also have adverse effects on human health. Inhaling HCl can damage the respiratory tract and have negative impacts on human health[20]. During the emission of HCl, it can react with other substances to form dioxins, which are organic compounds with strong biological toxicity. Dioxins are 130 times more toxic than cyanide and 900 times more toxic than arsenic. Dioxins have irreversible teratogenic, carcinogenic and mutagenic toxicity, and are regarded as one of the most dangerous chemicals in the world[21, 22]. Therefore, the application

of combustible solid waste as an alternative fuel is limited. Addressing the issue of HCl emissions is crucial. There are typically three main methods for removing HCl: pre-dechlorination, dechlorination in the furnace and dechlorination of flue gas[23-26]. Among these methods, dechlorination of flue gas is a conventional and effective method, which includes wet, semi-dry and dry method. The dry method is the most commonly used in power plants and garbage disposal incinerators due to its high efficiency, easy operation, and low cost [27, 28]. The most common method of dry dechlorination is to spray adsorbents, such as CaO and Ca $(OH)_2$, into the flue gas or pass the flue gas through adsorbents to achieve dechlorination at temperatures below 150 ^oC[29, 30]. Adsorbent and reaction temperature are key parameters during dechlorination and the reaction temperature is determined by the active temperature range of adsorbent, so the selection of adsorbent is extremely important. Traditional adsorbents have limitations, such as a fast failure time, low adsorption capacity per unit, poor thermal stability[31-33]. Therefore, to improve the performance of dechlorination, it is very important to choose a suitable material.

Hydrotalcite is a type of double hydroxyl compound metal oxide with a layered structure, possessing acid-base bifunctionality, exchangeability of interlayer anions, thermal stability, memory effect, and other properties. The chemical composition of hydrotalcite can usually be expressed as $[M_{1-x}^{2+} M_x^{3+} (OH)_2]^{x+}(A^{n-})_{x/n}\cdot mH_2O$. Among them, M^{2+} is divalent metal cations such as Mg^{2+}, Ni^{2+}, Co^{2+}, Zn^{2+}, Cu^{2+}; M^{3+} refers to trivalent metal cations such as Al^{3+}, Cr^{3+}, Fe^{3+}, etc; A^{n-} refers to inorganic and organic ions anions, such as CO_3^{2-}, NO^{3-}, Cl^-, OH^-, SO_4^{2-}, PO_4^{3-}, $C_6H_4(COO)^{2-}$, and complex ions[34-36]. Different interlayer anions can cause variations in the interlayer spacing and characteristics of hydrotalcite. The hydrotalcite with a complete structure can be obtained when the x value is between 0.17 and 0.33, which corresponds to a molar ratio of $M^{3+}/(M^{2+}+M^{3+})$ between 0.17 and 0.33. The most typical hydrotalcite is magnesium aluminum carbonate hydrotalcite (Mg-Al-CO_3), with a molar ratio of Mg/Al of 3[37]. Due to the special structure, hydrotalcite has been applied in catalysis, medicine, adsorption, and other fields[38-40].

Hydrotalcite is an effective material as an adsorbent in the treatment of heavy metals, chlorine and fluorine in wastewater[41], the removal of NO_x and SO_x in flue gas[42, 43], the capture of CO_2 [12, 34, 44]and other applications. Additionally, hydrotalcite can also be used to remove HCl gas from flue gas. Previous research has studied the effects of the molar ratio of Mg/Al, gas flow, and

HCl concentration on the HCl removal performance of Mg-Al-CO_3 hydrotalcite or loaded Mg-Al-CO_3 hydrotalcite. The results showed that the performance of Mg-Al-CO_3 hydrotalcite in removing HCl increased as the molar ratio of Mg/Al, pH, and HCl concentration increased[45, 46]. However, the characteristics of Mg-Al-CO_3 after calcination modification and the effect of calcination modification on HCl removal rate of Mg-Al-CO_3 hydrotalcite have not been clearly investigated. In addition, the characteristics and mechanism of HCl gas removal by calcined Mg-Al hydrotalcite are still unclear and need further analysis.

Therefore, in order to achieve higher performance adsorption in future plants, the effect of calcination modification on HCl gas removal performance of Mg-Al-CO_3 has been the focus of the current work. A wide temperature range, from 300 to 700 ^oC, was chosen for experiments to explore opportunities of process optimization and waste heat utilization in the flue gas. Firstly, a Mg-Al-CO_3 with a molar ratio of Mg/Al=3 was prepared using the coprecipitation method. Then the effects of different conditions on HCl removal by Mg-Al-CO_3 and calcined Mg-Al were studied. Finally, the characterization instruments and adsorption kinetics were employed to analyze the characteristics and reaction mechanism of HCl removal for Mg-Al-CO_3 and all calcined Mg-Al adsorbents.

2 Experiment material and methods

2.1 Experimental material

Mg $(NO_3)_2 \cdot 6H_2O$, Al $(NO_3)_3 \cdot 9H_2O$, NaOH and Na_2CO_3 with analytically pure grade were ordered from Sinopharm Chemical Reagent Co., Ltd. N_2 cylinder with 99.999 % grade and HCl cylinder with 2000 ppmv were ordered from Nanjing Special Gas Plant Co., Ltd.

2.2 Preparation and calcination

2.2.1 Mg-Al-CO_3 Preparation

The Mg-Al-CO_3 hydrotalcite intercalated with CO_3 was prepared using the coprecipitation method, as shown in Fig. 1. Based on the molar ratio of Mg/Al=3, $[OH^-]=2([M^{2+}]+[M^{3+}])$ and $2[CO_3^{2-}] = [M^{3+}]$, two nitrates (Mg $(NO_3)_2 \cdot 6H_2O$ and Al $(NO_3)_3 \cdot 9H_2O$) and two bases (NaOH and Na_2CO_3) were weighed, then two nitrates and two bases were dissolved into ultra-pure water at 60 ^oC, respectively. Both mixed solutions were added to a four-neck flask by peristaltic pump at 60 ^oC, during this process, the pH value kept at 11-11.5, and agitator speed was maintained at 300 r /min

in flask. The obtained new substance was then stirred for 2 hours at 60 °C. The Mg-Al-CO_3 was prepared after the new substance grew crystals for 20 hours at 80 °C. The solid part was washed until neutral, dried and grounded. Particle sizes ranging from 40 to 60 mesh were chosen for subsequent experiments. Ultra-pure water was used throughout the preparation process.

2.2.2 Mg-Al-CO_3 calcination

The Mg-Al-CO_3 sample was calcined for 2h in a muffle furnace at 400, 500, 600 and 700 °C, respectively. The resulting samples were designated as Mg-Al-T, where T represents calcined temperature.

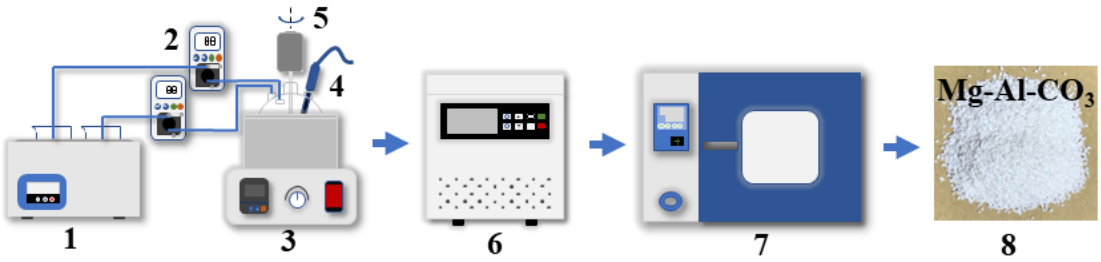

1. Thermostatic water pot; 2. Peristaltic pump; 3 Thermostatic oil pot; 4. pH meter; 5. Mixer; 6. Centrifuge; 7. Drying oven; 8. Mg-Al-CO_3 hydrotalcite

Fig. 1 Preparation process of Mg-Al-CO_3 hydrotalcite

2.3 Characterization

The physicochemical characteristics of Mg-Al-CO_3 were characterized using several techniques, including ICP-OES, XRD, SEM, TGA, and a specific surface area and porous size analyzer. The concentrations of Mg^{2+} and Al^{3+} were measured by ICP-OES (Agilent 5110) from Agilent Technologies, Inc. XRD analysis was performed using a Bruker D8 ADVANCE equipment from Bruker Daltonics Inc., Germany, with a range of diffraction angle from 5-80 ° and a step size of 0.08 °. The surface topography was analyzed using SEM S4800 from Hitachi Limited, Japan. The specific surface area and pore structure were analyzed using the specific surface area and pore size analyzer ASAP 2460 from Micromeritics Instruments Corporation, America, and the specific surface area and pore size distribution were calculated by Brunauer-Emmet-Teller (BET) linear regression equation and Barrett-Joyner-Halenda (BJH) method[47], respectively. The thermal stability of Mg-Al-CO_3 was analyzed using a thermogravimetric analyzer STA 8000 from

PerkinElmer, Inc., America.

2.4 Experimental equipment and methods

2.4.1 Experimental equipment

The self-building experimental platform consisted of four components: the gas system, reactor system, data acquisition system, and gas treatment system, as shown in Fig. 2. The gas system was used to control gas flow and initial concentration of HCl. The mass flowmeter used was HORIBAMETRON S49-33/MT from Beijing HORIBA METRON Instruments Co., Ltd., China. The reactor system consisted of a furnace and a quartz tube with an inner diameter of 10 mm. The data acquisition system was comprised of an LJR-600 condenser and a HCl analyzer (Model 7900FM HCl GFC) from Signal Group Ltd., Britain. The main function of the gas treatment system was to adsorb HCl gas and avoid environmental pollution.

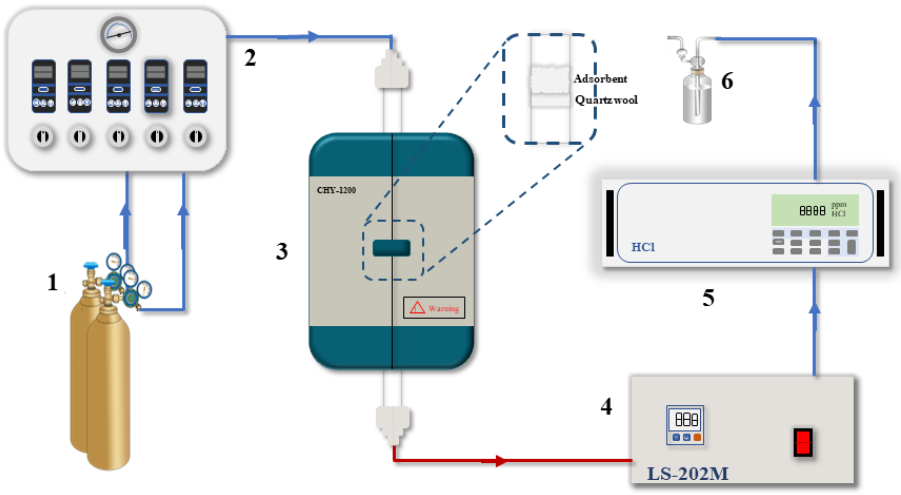

1. Gas cylinder; 2. Mass flowmeter; 3. Reactor; 4. LJ-202M condenser; 5. HCl analyzer; 6. Gas-washing bottle

Fig. 2 Experimental schematic diagram

2.4.2 Experimental process

Firstly, the adsorbent was placed in the middle of the reactor, the leakage test of system was checked with N_2; then the reactor was pre-heated to a certain reaction temperature in an inert condition using N_2. After reaching the reaction temperature, a gas mixture containing 400 ppmv HCl and carrier gas N_2 was introduced to the reactor, and the data on HCl concentration of the outlet stream were collected by the HCl analyzer. The experiment was considered complete when the HCl concentration returned to its initial level. Finally, the system was shut

down and then cooled down, the reactive adsorbent was collected for further analysis. The HCl analyzer used in the experiments is capable of real-time data recording at an interval of 1 second. To ensure the accuracy and reliability of the data, we utilized the raw data for analyzing the HCl removal rate. Additionally, for the purpose of visual clarity, we will plot the original data at specific intervals of 14 minutes. The detailed experimental conditions are shown in Table. 1.

Table. 1 Experimental condition

Parameters	Unit	Conditions
Adsorbent	/	Mg-Al-CO_3, Mg-Al-400, Mg-Al-500, Mg-Al-600, Mg-Al-700
Particle diameter	mesh	40-60
Reaction temperature	°C	300, 400, 500, 600, 700
Calcination temperature	°C	400, 500, 600, 700
HCl concentration	ppmv	400
Quality	g	0.5
Gas	/	HCl, N_2
Gas flow	L/min	0.5

2.4 Performance indexes

The instantaneous HCl removal rate is calculated by Eq. 1.

$$\eta = \frac{C_{\text{in}} - C_{\text{out}}}{C_{\text{in}}} \times 100\% \quad \text{Eq. 1}$$

Where η is the instantaneous removal of HCl rate at t time, %. C_{in} and C_{out} are the HCl concentration of inlet and outlet, respectively, ppmv.

The average removal of HCl rate is calculated by Eq. 2.

$$\overline{\eta} = \frac{1}{N}\sum_{i=1}^{N}\eta_i \quad \text{Eq. 2}$$

Where $\overline{\eta}$ is the average HCl removal rate, %. N is the test time. η_i is the instantaneous HCl removal rate at the t time, %.

The breakthrough chlorine capacity is defined as the total mass of HCl adsorbed per unit mass of adsorbent from the beginning of the reaction until the time of complete breakthrough. The breakthrough chlorine capacity is calculated by Eq. 3.

$$Q_t = 10^{-3}\int_0^t \frac{36.5(C_0 - C_1)V_s}{22.4m}dt \quad \text{Eq. 3}$$

Where Q_t is the breakthrough chlorine content， mg/g. V_s is the volume flow of reaction gas, L/min.

m is the adsorbent quality, g.

The Intra-particle diffusion model is usually used to determine whether diffusion is the only rate control step of a reaction. The equation is given by Eq. 4[48],

$$q_t = k_1 t^{1/2} + C \quad \text{Eq. 4}$$

Where q_t is the adsorption capacity of adsorbent at time *t*, mg·g^{-1}. k_1 is the rate constant of intragranular diffusion model, mg· (g·min$^{-1/2}$)$^{-1}$. *C* is constant, mg·g^{-1}.

The pseudo-first-order model is used to judge whether the adsorption process is controlled by diffusion or surface reaction, when adsorption is controlled by chemical adsorption of chemical factors, the equation is described by Eq. 5,

$$\log(q_e - q_t) = \log q_e - \log(\frac{k_1}{2.303}) \quad \text{Eq. 5}$$

Where q_e represents HCl equilibrium adsorption amount, mg · g^{-1}. q_t is the HCl adsorption capacity at time *t*. k_1 is the rate constant, min^{-1}.

The pseudo-second-order (PSO) model is based on the assumption that the adsorption rate is controlled by a chemical adsorption mechanism, which involves electron sharing or electron transfer between the adsorbent and the adsorbate. The equation is written as Eq. 6[49],

$$\frac{t}{q_t} = \frac{1}{k_2 q_e^2} + \frac{1}{q_e} \quad \text{Eq. 6}$$

Where q_e represents HCl equilibrium adsorption capacity, mg · g^{-1}. q_t is the HCl adsorption capacity at time *t*. k_2 is the rate constant, min^{-1}.

The Elovich model is commonly used for the chemical adsorption of gases on solid surfaces. The Elovich model is defined by Eq.7,

$$q_t = (\frac{2.3}{k_0}) \lg(t + t_0) - (\frac{2.3}{k_0}) \lg t_0 \quad \text{Eq.7}$$

Where $t_0 = 1/k_0 k_f$. k_0 is the initial adsorption rate at q_t = 0, mg /g·min. k_f is desorption constant, g·mg. Eqs. 8 is simplified with $tk_0k_f << 1$, t=0, q_t=0.

$$q_t = k_0 \ln(k_f k_0) + k_0 \ln(t) \quad \text{Eq. 8}$$

The Bangham model is used to describe pore diffusion, which optimizes the Lagergren model through time compensation, making it well suited in predicting the adsorption process of various

adsorbents. The model function is shown in Eq. 9[50],

$$\lg\{\lg[q_e/(q_e-q_t)]\} = \lg(\frac{k_2}{2.303}) + n\lg t \quad \text{Eq. 9}$$

Where q_e is the HCl equilibrium adsorption capacity, g·min. k_2 is the Bangham rate constant. q_t is HCl adsorption capacity at the t time.

3 Results and Discussion

3.1 Mg-Al-CO_3 hydrotalcite characteristic

According to the results of ICP-OES, the molar ratio of Mg/Al was 3.1, which satisfied the preparation requirements. Fig. 3A and B show the XRD pattern and SEM image, respectively, of the original Mg-Al-CO_3 with a Mg/Al ratio of 3. In Fig. 3A, there are the characteristic diffraction peaks of hydrotalcite (PDF- # 35-0965) in Mg-Al-CO_3, with the 2θ values of 11.36°, 22.88°, 34.44°, 38.38°, 45.42°, 60.46°, 61.74° corresponding to hydrotalcite crystal faces of (003), (006), (012), (015), (018), (110), (113), respectively. The layer spacing of d_{003} in Mg-Al-CO_3 is 0.778 nm. It can be seen from the XRD curve that the diffraction peaks of Mg-Al-CO_3 posed a narrow peak pattern and high intensity, indicating that the prepared Mg-Al-CO_3 had the characteristics of single crystal phase, high crystal plane order, good crystallinity and complete crystal form. These results were consistent with those reported in previous studies[51, 52]. Fig. 3B shows that Mg-Al-CO_3 has a regular hexagonal lamellar structure, with the wide and thickness of layered Mg-Al-CO_3 being around 300-500 nm and 50nm, respectively. The above results indicate that the preparation conditions are conducive to nucleation and growth of crystals, and the layered structure of Mg-Al-CO_3 hydrotalcite was successfully prepared.

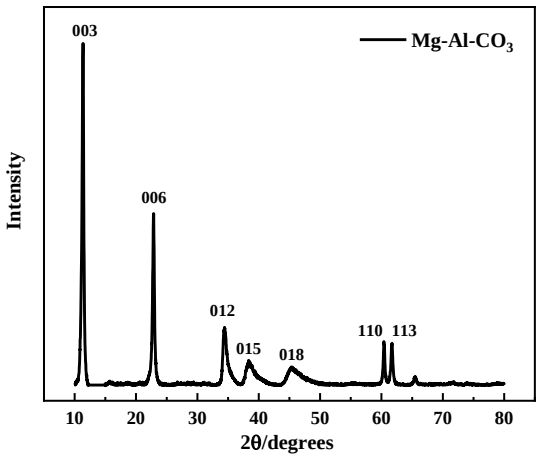

A. XRD pattern

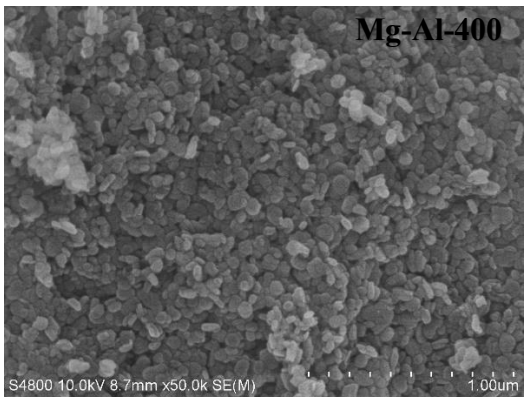

B. SEM image

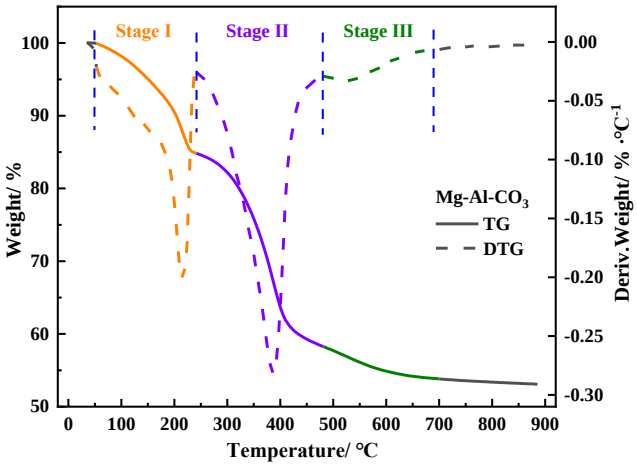

C. The TG/DTG curve in N_2

Fig. 3 The XRD patterns, SEM images, and TGA of Mg-Al-CO_3

To further investigate the properties of Mg-Al-CO_3, its thermal stability was studied. The thermogravimetric curve, shown in Fig. 3C, was obtained with a heating rate of 10 °C /min over a temperature range of 35 to 900 °C. The curve reveals that the weight of Mg-Al-CO_3 decreased as the temperature rose, and the weight loss tended to stabilize at 700 °C with a final reduction of 47%. In the DTG curve, there were three weight loss stages. Stage I occurred between 55 and 240 °C, with a weight loss of 15.4 %, where the water content was lost first, followed by the interlayer water as the temperature increased. The maximum weight loss rate occurred at 215 °C. The release of interlayer water developed pores of Mg-Al-CO_3. The maximal weight loss of 26.8 % was observed in stage Ⅱ when the temperature was between 250 and 480 °C. The peak value was at 400 °C and the weight loss rate was at its maximum. More water was lost and the interlayer CO_3^{2-} started to convert to CO_2 and was subsequently released, therefore, the pore structure was further developed. Stage Ⅲ occurred from 500 to 700 °C, with a weight loss of only 4 %. In this stage, the CO_3^{2-} was completely converted to CO_2, and the ordered layered structure of Mg-Al-CO_3 was destroyed, bimetallic composite oxides were formed.

3.2 Calcinated Mg-Al adsorbents characteristic

The XRD patterns and SEM images of calcined Mg-Al adsorbents are shown in Fig. 4. In Fig. 4A, it can be observed that after calcination, the characteristic diffraction peak of hydrotalcite almost disappeared, new peaks of magnesium aluminum mixture ($Mg_xAl_yO_z$) were generated, and the peak intensity of $Mg_xAl_yO_z$ increased with the increasing calcination temperature, $MgAl_2O_4$ was the main

component in $Mg_xAl_yO_z$. The calcined Mg-Al-CO_3 can be described by *React.*1[38].

$$Mg_{3n}Al_n(OH)_{8n}(CO_3)_{n/2}\bullet mH_2O \rightarrow Mg_{3n}Al_nO_{9n/2} + (n/2)CO_2 + (m+4n)H_2O \quad (React.\ 1)$$

As shown in Fig.4B, the morphology of Mg-Al-400 appeared to be favorable. In comparison to the SEM image of Mg-Al-CO_3 (Fig.3 B), the morphology of calcined Mg-Al adsorbents exhibited minimal agglomeration, and displayed an even distribution. Combined with the TGA from Fig. 3C, in this stage, only the water and partly interlayer were released. When calcination temperature with was more over 400 ºC, calcined Mg-Al adsorbents were sintered and destroyed gradually. The sintering phenomenon of Mg-Al-500 became more obvious, even worse in Mg-Al-600 and Mg-Al-700. According to TGA results, at this stage, the CO_3^{2-} was completely released and the layered structure of Mg-Al-CO_3 was destroyed.

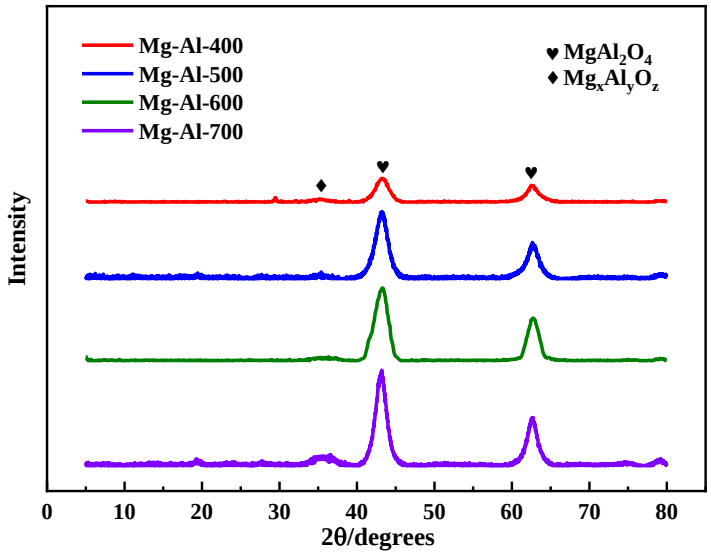

A.XRD patterns

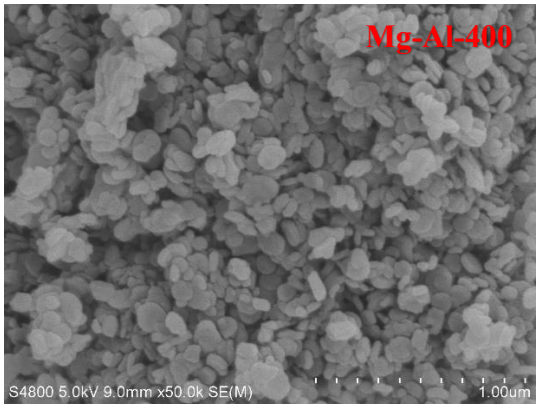

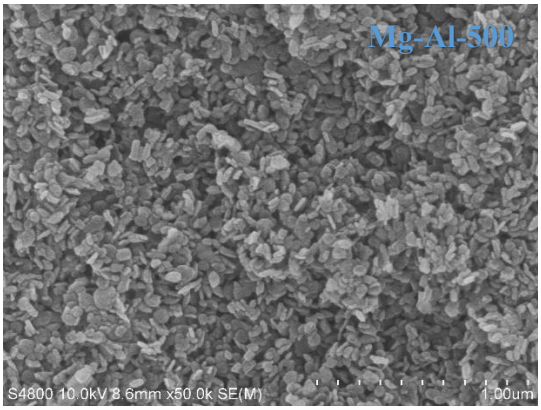

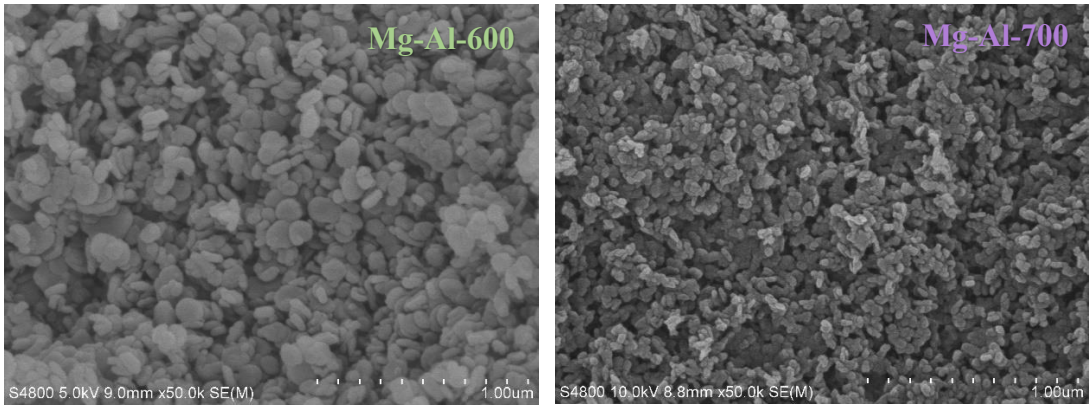

B. SEM images

Fig. 4 The XRD patterns and SEM images of calcined Mg-Al adsorbents

3.3 The effect of reaction temperature on removing HCl performance

Fig. 5A shows HCl removal rate using Mg-Al-CO_3 when the temperature increased from 300 to 700 ºC with an initial HCl concentration of 400 ppmv. It can be observed that the effectiveness and the reaction time of HCl removal decreased rapidly with the increase of reaction temperature. The HCl removal rate initially increased and then decreased over the first 120 minutes of the experiment. The highest HCl removal rate was observed at a reaction temperature of 400 ºC, which was better than the removal rates obtained at other reaction temperatures. In Fig. 5B, it can be seen that within the first 120 minutes, the average removal rate of HCl initially increased from 80.89% to 83.83%, with an increase of 3.6%, and subsequently decreased from 83.83% to 45.28%, resulting in a decrease of 45.99%. The phenomenon shows that increasing the reaction temperature has a positive effect on improving HCl removal rate. This phenomenon may be attributed to the decomposition of the interlayer anion CO_3^{2-}, resulting in the generation of gaseous CO_2. The released CO_2 developed the pores of Mg-Al-CO_3, thereby promoting the adsorption capacity of Mg-Al-CO_3. However, when the reaction temperature exceeded 400 ºC, the structure of Mg-Al-CO_3 may be destroyed, the morphology of calcined Mg-Al adsorbents is shown in Fig. 4B, leading to a decrease in HCl removal performance. In addition to the HCl removal rate and the breakthrough time, the breakthrough

chlorine capacity is also an important index to evaluate the dechlorination performance of adsorbents.

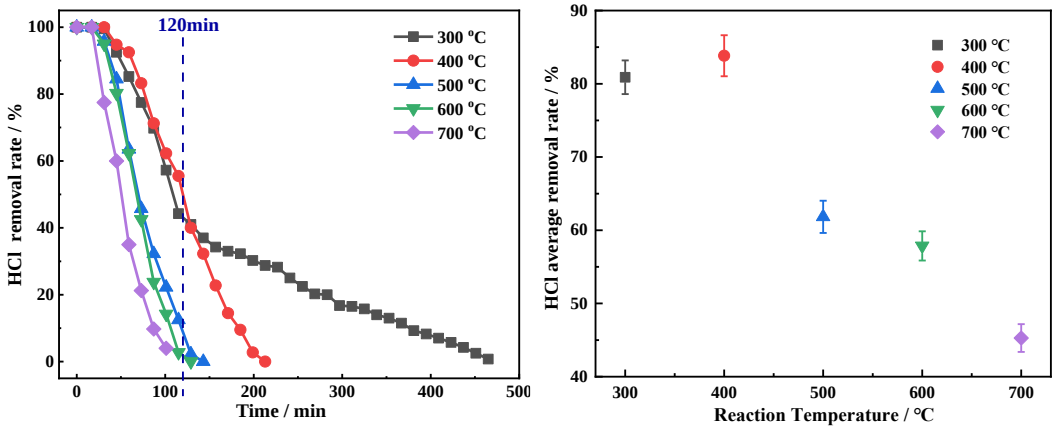

A. The instantaneous HCl removal rate B. The average HCl removal rate within first 120 min

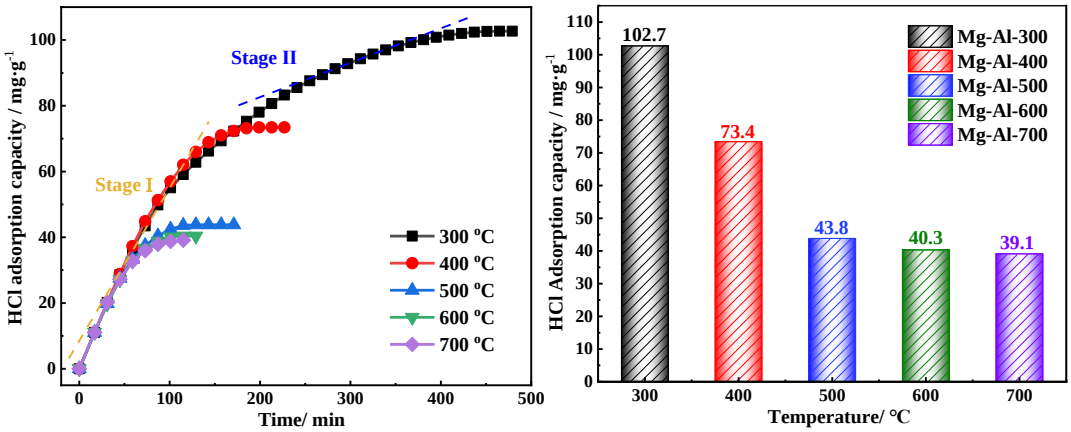

C. The adsorption chlorine capacity curves D. The breakthrough chlorine capacity

Fig.5 HCl removal rate and the adsorption chlorine capacity at different reaction temperatures

Fig. 5C and D show the adsorption curves of adsorbing HCl by Mg-Al-CO_3 at different reaction temperatures. With the increasing reaction temperature, the adsorption capacity of Mg-Al-CO_3 reduced, following a similar trend to that of the HCl removal rate. In Fig.5C, it is apparent that the process of adsorption can be divided into two stages. Stage I is a rapid adsorption process at the beginning of the adsorption. Thus, the effect of adsorption by Mg-Al-CO_3 is the best and the adsorption chloride capacity increased rapidly. After stage I is completed, there is a saturated zone in adsorbent, therefore, the adsorption rate slows down in stage Ⅱ, and this process continues until the adsorption capacity becomes saturated. As seen in Fig. 5D, the adsorption capacity decreased from 102.7 mg g^{-1} to 39.1 mg g^{-1} with increasing reaction temperature. Compared with the

adsorption chlorine capacity at 400 °C, the adsorption chlorine capacity increased 29.3 mg g^{-1} at 300 °C. Although the adsorption chlorine capacity at 400 °C is better than that of other reaction temperatures within the reaction time range of 0 to 120 min, the adsorption chlorine capacity at 300 °C is ultimately the better option.

The main reasons are that according to the TG/DTG curve, the weight of Mg-Al-CO_3 decreased by decomposition of carbonate to carbon dioxide with increasing temperature, indicting a reduction in the number of substances participating in the reaction. When the temperature rises from 300 to 400 °C, leads to a more decrease in effective dechlorination components, resulting in a lower breakthrough chlorine capacity as the temperature increases.

However, the release of carbon dioxide enriches the pore structure of the material and increases its specific surface area. The enhanced pore structure facilitates the entry of HCl into the internal reaction through the pore channels, while the increased specific surface area provides more reactive sites, thereby improving the reaction rate. As a result, in the early stages, the HCl removal rate at 400 °C is better than that at 300 °C. Since the number of magnesium involved in the reaction does not change while the number of carbonates involved in the reaction decreases, the development of pores and the increase in specific surface area only contribute to an increase in the reaction rate, rather than the adsorption capacity.

3.4 The effect of calcined temperature on removing HCl rate

Fig. 6A and B show the HCl removal rates of Mg-Al-CO_3 and calcined Mg-Al adsorbents at an HCl concentration of 400 ppmv, a reaction temperature of 300 °C, and a gas flow of 500 ml/min. As the calcination temperature increased from 400 to 700 °C, the efficiency of HCl removal reduced. Among the calcined Mg-Al samples, only Mg-Al-400 showed better HCl removal performance than Mg-Al-CO_3. Additionally, the breakthrough time of Mg-Al-400 increased by 47 min, representing a 27% increase. In order to further illustrate the effect of calcinating modification on efficiency of removing HCl, the average HCl removal rate was studied within the first 120 min in Fig. 6B. The average HCl removal rate of calcined Mg-Al adsorbents rapidly decreased from 90.11% to 43.42% when the calcination temperature rose from 400 to 700 °C. In comparison toMg-Al-CO_3, the average HCl removal rate of Mg-Al-400 increased by 11.7%. However, the dechlorination performance of Mg-Al-500, Mg-Al-600 and Mg-Al-700 was not as effective as that of Mg-Al-CO_3 and worsened

with increasing calcination temperature.

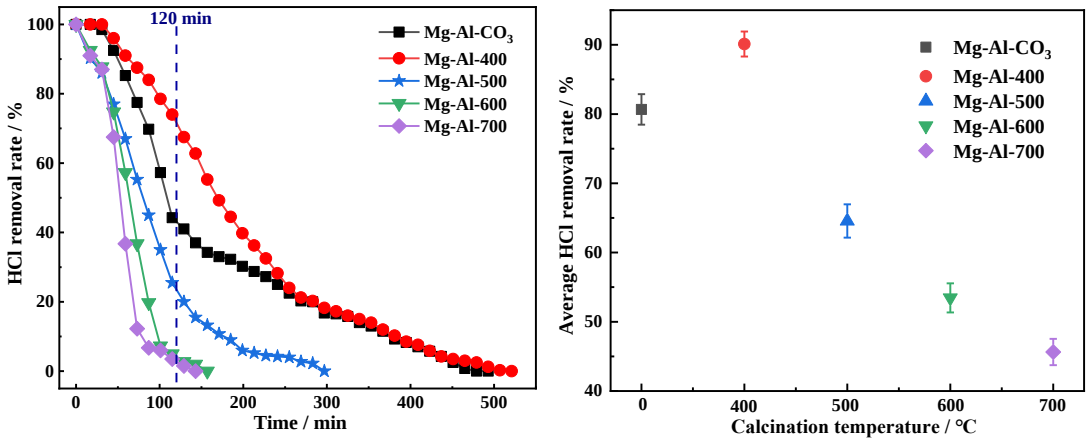

A. The instantaneous HCl removal rate B. The average HCl removal rate within first 120 min

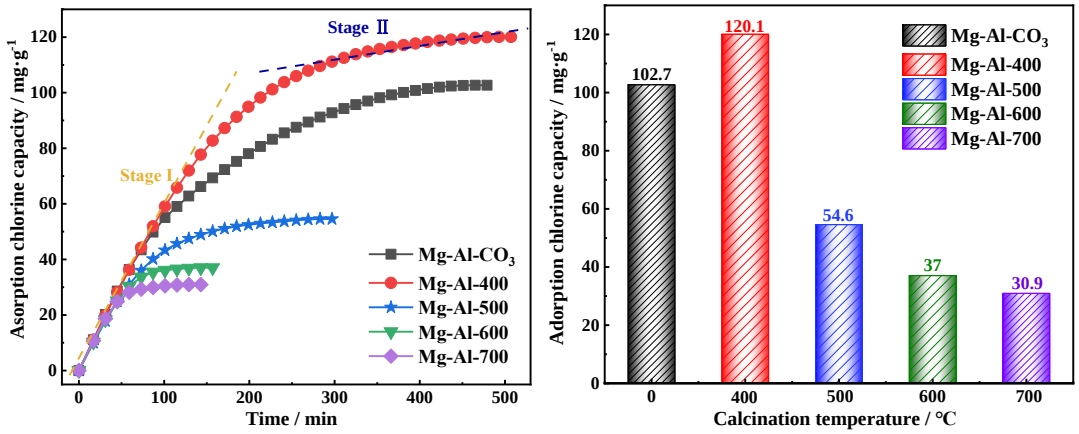

C. The adsorption chloride capacity curves D. The breakthrough chloride capacity

Fig. 6 HCl removal rate and the adsorption chlorine capacity of Mg-Al-CO_3 and calcined Mg-Al adsorbents

The curves of adsorption chlorine capacity and breakthrough chlorine capacity are shown in Fig. 6C and D. In Fig. 6C, with the increase of calcination temperature, the adsorption chlorine capacity of calcined Mg-Al adsorbents decreased, the reaction time required to reach breakthrough chlorine capacity also deceased. It is worth noting that among the calcined Mg-Al adsorbents, only Mg-Al-400 exhibited a better adsorption chlorine capacity compared to Mg-Al-CO_3. It can also be seen from Fig. 6C that the adsorption process could also be divided into two stages. The first stage was the rapid adsorption stage, in which HCl was rapidly adsorbed by the adsorbents, and Mg-Al-400 had the longest reaction time. The second stage was the slow adsorption stage, where the adsorption chlorine capacity of adsorbents tended to be saturated, the slope of adsorption curves decreased, and

the adsorption rate slowed down. The breakthrough chlorine capacity is shown in Fig. 6D. The breakthrough chlorine capacity of Mg-Al-CO_3 was 102.7 mg g^{-1}, while the breakthrough chlorine capacity of Mg-Al-400 was 120.1 mg g^{-1}, which was 1.17 times that of Mg-Al-CO_3. However, the breakthrough chlorine capacity decreased with increasing calcination temperature, and the breakthrough chlorine capacity of Mg-Al-700 was 30.9 mg g^{-1}, which was only 0.3 times that of Mg-Al-CO_3. Under similar working conditions (170°C and 300 ppmv HCl), Mg-Al-400 exhibits superior performance compared to Mg-Al layered double hydroxides[45]. In another research study, it was found that the breakthrough chloride capacity of Mg-Al-400 increases by approximately 5-10% when compared to materials including HN-1, HK-1, and HK-1S at temperatures ranging from 300 to 500 °C and an HCl concentration of 2500 ppmv[53]. This indicates that Mg-Al-400 shows enhanced dechlorination capabilities in comparison to these specific materials under the specified operating conditions.

3.5 The effect of flow rate on removing HCl rate by Mg-Al-400

The HCl removal rate of Mg-Al-400 is shown in Fig. 7 A and B. The experiments were conducted at a flow rate ranging from 0.5 to 2.0 L min^{-1}, with an initial HCl concentration of 400 ppmv, and a reaction temperature of 300 °C. The instantaneous HCl removal rate and reaction time decreased rapidly. The best performance of removing HCl was observed at a flow rate of 0.5 L/min. In the Fig. 7B, the maximal HCl average removal rate of Mg-Al-400 was achieved at a flow rate of 0.5 L/min. As the flow rate increased from 0.5 to 2 L/min, the HCl average removal rate decreased from 90.11% to 45.16%, resulting in a reduction of 44.95%, indicating that higher flow rate had a negative effect on HCl removal rate of Mg-Al-400.

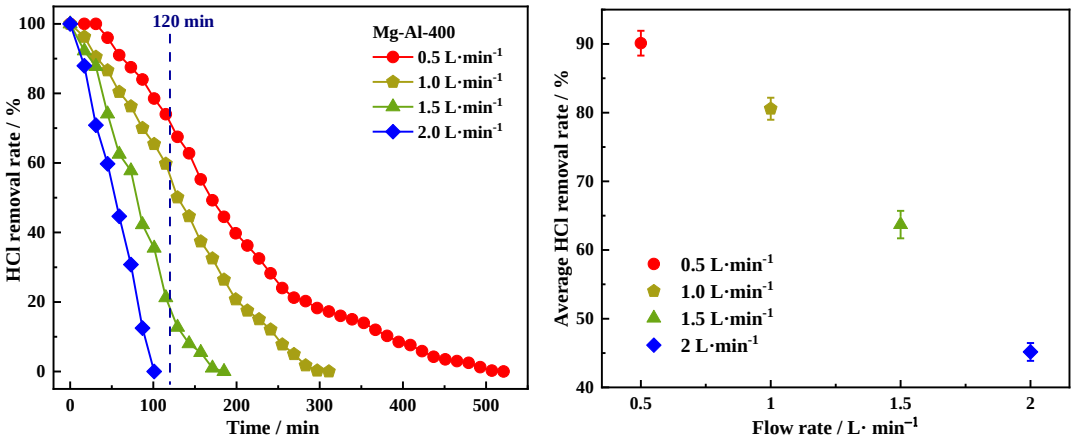

A. The instantaneous HCl removal rate B. The average HCl removal rate within first 120 min

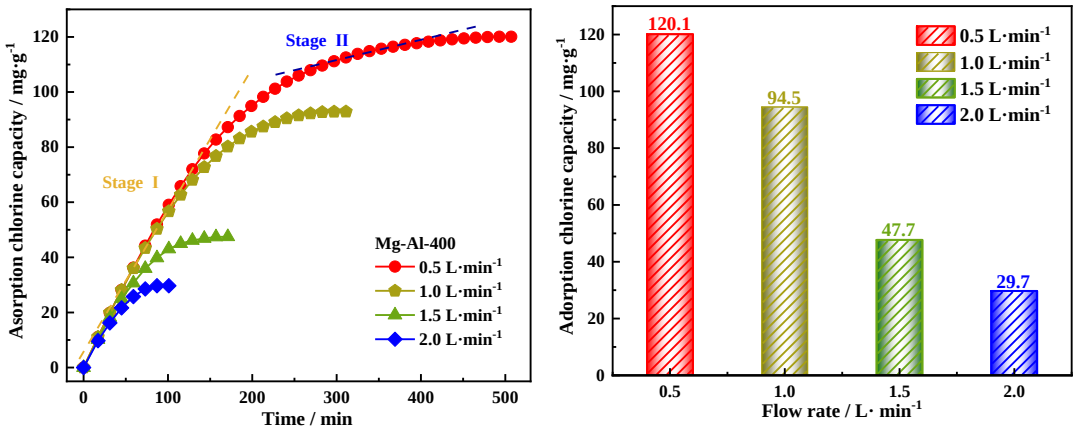

C. The adsorption chloride capacity curves D. The breakthrough chloride capacity

Fig.7 HCl removal rate and the adsorption chlorine capacity of Mg-Al-400

Fig. 7 C and D show the adsorption chloride capacity curves and the breakthrough chloride capacities. In Fig. 7C, the process of adsorption included two stages, which were fast adsorption process and slow adsorption process. The adsorption processes were finished faster with the increase of gas flow rate. It can be seen from Fig. 7D that the breakthrough chloride capacity reduced from 120.1 to 29.7 mg g^{-1}. The main reason is that the reaction time of adsorbents with HCl decreased as the flow rate of the gas increased. This leads to an increased amount of HCl being treated per unit mass of adsorbent per unit time, which ultimately results in a reduction in the performance of Mg-Al-CO_3.

3.6 The characterization and mechanism

As can be seen from the results of specific surface area and pore structure analysis in Fig. 8A-C, according to the International Union of Pore and Applied Chemistry (IUPAC), six categories, six hysteresis loop categories and three pore categories were defined: 0-2 nm for micropores, 2-50 nm for mesopores, and greater than 50 nm for macropores[47, 54]. The adsorption/desorption curves of adsorbents exhibited a category Ⅴ curve and H3 hysteresis loop, where the hysteresis loop was caused by capillary condensation, and the H3 hysteresis loop was a typical hysteresis loop caused by the layered structure. As shown in Fig. 8B, the pore size of Mg-Al-CO_3 was mainly fell within

the mesopore range, with a small number of pores, and an average pore diameter of 30.57 nm, the specific surface area was 66.35 m^2 g^{-1}. The pore size of calcined Mg-Al samples was mainly concentrated in the mesopore range (2-50 nm), and the number of pores increased. When the calcination temperature rose from 400 to 700 °C, the quantity of mesopores decreased, while the number of macropores increased. As a result, the average pore diameter increased from 14.36 to 23.3 nm, and the specific surface area decreased from 183.73 m^2 g^{-1} to 130.53 m^2 g^{-1}, representing a 29% decrease. The highest specific surface area was achieved at 400 °C, reaching a value of 183.73 m^2 g^{-1}. Compared to Mg-Al-CO_3, the specific surface area of Mg-Al-400 increased by 352 %. The results showed that the porous structure of calcined Mg-Al samples was significantly developed, and the optimum calcination temperature was found to be 400 °C. The larger specific surface area and porous structure can provide more active sites, facilitating the diffusion of adsorbates and promoting both physical and chemical reactions (as shown in Fig. 9). This also explains why Mg-Al-400 has the best performance in removing HCl. Interestingly, it can be seen from Fig. 8C that the specific surface area and porous structures of Mg-Al-500, Mg-Al-600, and Mg-Al-700 also were better than those of Mg-Al-CO_3. To further explain why the HCl removal rate of Mg-Al-CO_3 was better than that of Mg-Al-500, Mg-Al-600, and Mg-Al-700, the XRD patterns of reaction products were analyzed and discussed.

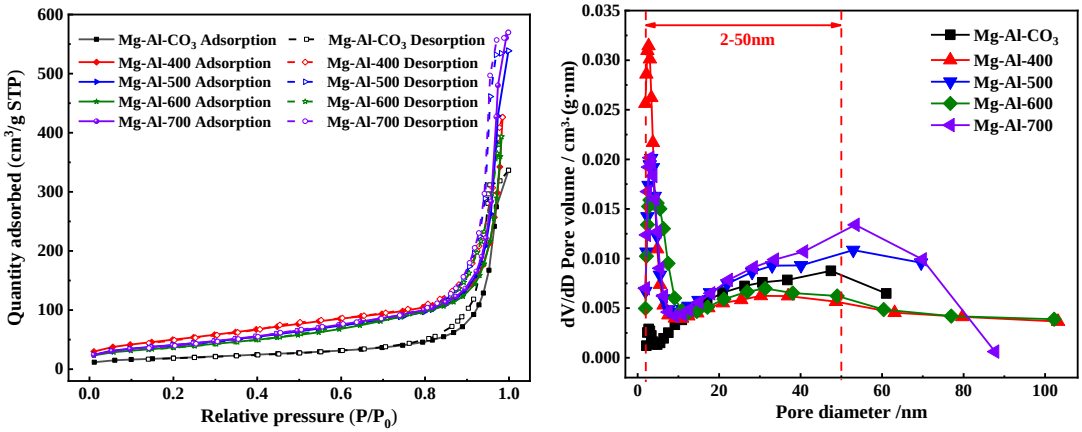

A. The adsorption/desorption curves B. The pore structure distribution curves

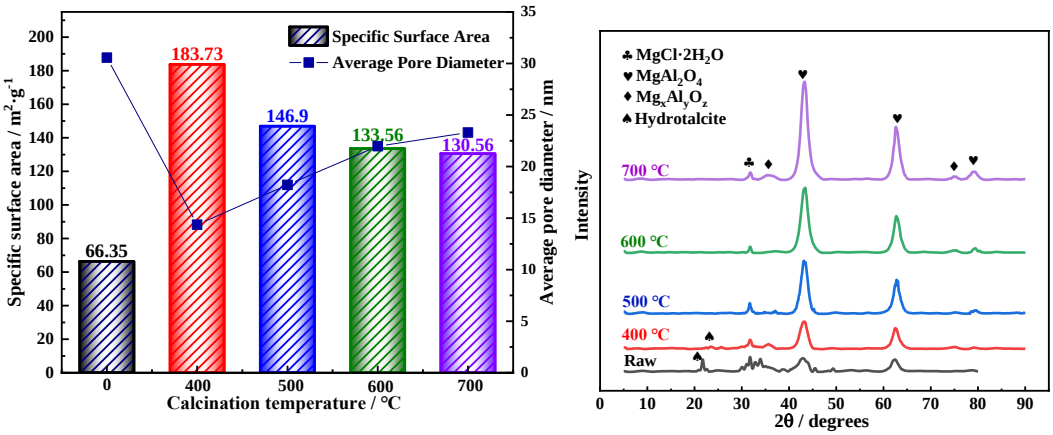

C. The pore structure of adsorbents D. The XRD patterns of adsorbents after reaction

Fig. 8 The specific surface area and pore structure, XRD patterns, and reaction paths of adsorbents

As shown in Fig. 8D, when comparing the XRD patterns to those shown in Fig.4A, it can be observed that $MgCl_2 \cdot 2H_2O$ was a new resultant in all reactions, indicating that Mg^{2+} was easy to react with Cl^-, as depicted in path 2 of Fig. 9, and was found to be the main chemical reaction pathway. Since Mg-Al-400 had the most favorable pore structure and a great number of reaction active sites, it exhibited the best performance in terms of HCl removal. Moreover, $Mg_xAl_yO_z$ remained the main product after the reaction, indicating that $Mg_xAl_yO_z$ had limited reactivity with HCl, and as the calcination temperature increased, the HCl removal rate of calcined Mg-Al adsorbents deteriorated. In addition, it can be seen from Fig. 8D that both Mg-Al-CO_3 and Mg-Al-400 had hydrotalcite characteristic peaks, indicating the presence of a hydrotalcite structure after the reaction. The reason for this phenomenon is that hydrotalcite can regenerate under appropriate conditions when the structure is not completely destroyed, and this feature is called “the memory”. According to the result of TGA, the Mg-Al-CO_3 was not completely decomposed when the calcination temperature was below 400 ºC. So, during the reaction, Cl^- can enter the layers of hydrotalcite to replace CO_3^{2-} or act as a supplementary anion. As a result, the new hydrotalcite (Mg-Al-Cl) was generated, where Cl^- was fixed in hydrotalcite[45, 46]. The chemical reaction equation

is shown in *React*. 2 and the reaction path is shown in path 3 in Fig. 9. While the hydrotalcite structure of Mg-Al-500, Mg-Al-600, and Mg-Al-700 destroyed, the reaction of path 3 could not be regenerated or was difficult to be regenerated. From the results of HCl removal, although calcined Mg-Al adsorbents exhibited a certain adsorption capacity through physical adsorption, the chemical pathway was the main adsorption mechanism. The results further elucidated the reason behind the superior HCl removal performance of Mg-Al-CO_3 compared to Mg-Al-500, Mg-Al-600, and Mg-Al-700. The above results demonstrated the occurrence of both physical and chemical reactions during the process of removing HCl, and the chemical reaction was the dominant one.

$Mg_{3n}Al_n(OH)_{8n}(CO_3)_{n/2}\bullet mH_2O + nHCl \rightarrow Mg_{3n}Al_n(OH)_{8n}Cl_n + (n/2)CO_2 + (m + n/2)H_2O$ *(React. 2)*

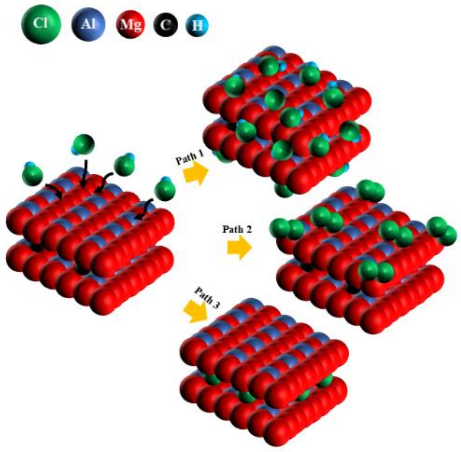

Fig. 9. Reaction paths of adsorbent

3.7 Apparent adsorption kinetic

The process of adsorption contains three steps, external diffusion, pore diffusion and surface reaction[55]. Adsorption kinetics mainly studies the diffusion performance of adsorbate within adsorbent particles by analyzing the relationship between the adsorption amount of adsorbent and adsorption time during the adsorption process, and explores the adsorption mechanism of adsorbent on the adsorbate. The conventional adsorption kinetic models, the intra-particle diffusion model, the pseudo-first-order model (PFO), the pseudo-second-order model (PSO), the Elovich model and the

Bangham model, were used to investigate the HCl removal by Mg-Al-CO_3 and calcined Mg-Al adsorbents under specific conditions, including a HCl concentration of 400 ppmv, a reaction temperature of 300 ºC, and a gas flow of 500 ml/min, and the results are shown in Fig. 10. The correlation coefficients (R^2) of the different adsorption kinetic models are listed in Table 2.

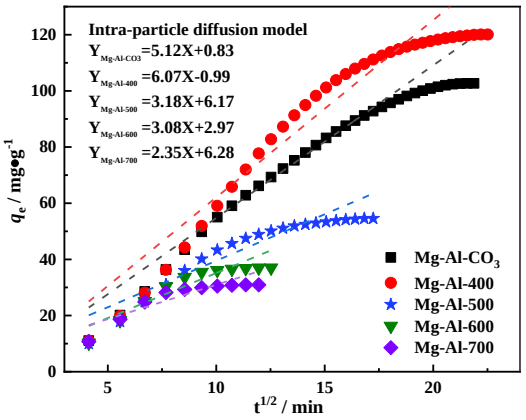

A. Intra-particle diffusion model

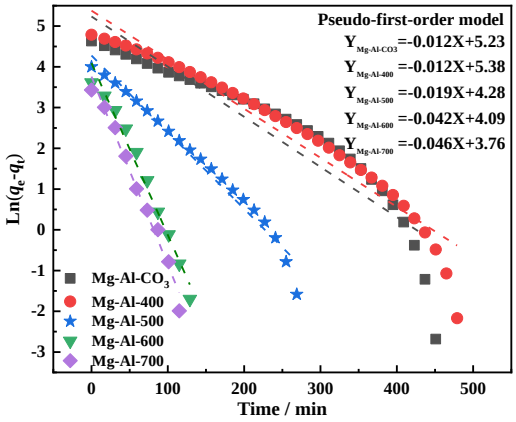

B. Pseudo-first-order model

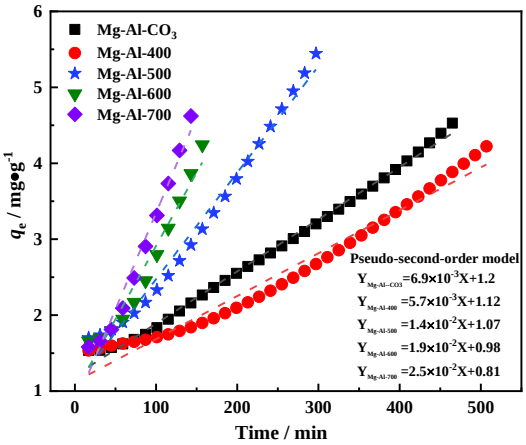

C. Pseudo-second-order model

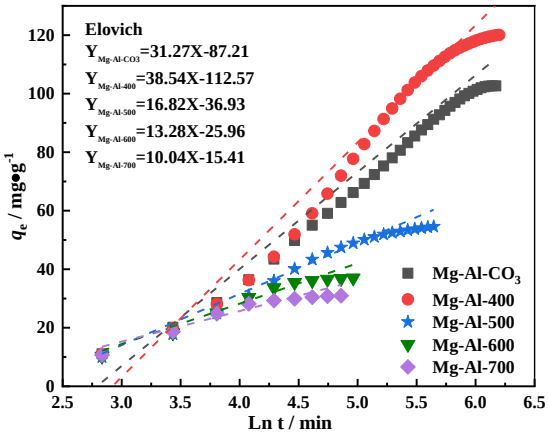

D. Elovich model

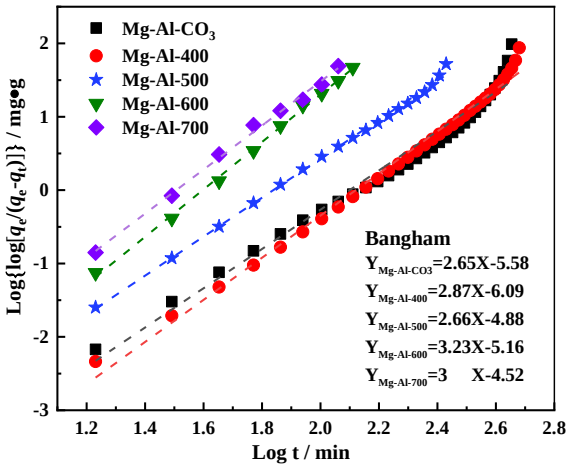

E. Bangham model

Fig. 10 The fitting results of different adsorption kinetic models

As shown in Fig. 10, combined with Table 2, the fitting results of R^2 showed that the matching of the intra-particle diffusion model was relatively low, and the fitting line did not pass through the origin, therefore, the adsorption reactions were likely controlled by multiple steps. The adsorption results were fitted poorly by PFO model, but the fittings of Mg-Al-500, Mg-Al-600, and Mg-Al-700 were relatively high, with R^2 values over 0.97. This suggested that the chemical reactions occurred on the surface of Mg-Al-500, Mg-Al-600, and Mg-Al-700 during the HCl removal process. The R^2 value of the Elovich model of adsorption was found to be greater than 0.9, indicating that chemical reaction occurred the adsorption process. Among the various adsorption kinetic models, the Bangham model and PSO model showed R^2 values higher than 0.97. The results demonstrated that chemical reacted with HCl occurring on the surface adsorption and involved electron sharing or electron transfer between the adsorbent and the adsorbate. The above results showed that the reaction of Mg-Al-CO_3 and calcined Mg-Al adsorbents with HCl was a complex process, and the process of the adsorption reaction was controlled by multiple steps. The results of the adsorption kinetic model were consistent with the experimental results obtained from the above analysis.

Table. 2 The correlation coefficients (R^2) of different adsorption kinetic models

Model	Intra-particle diffusion model	Pseudo-first-order model	Pseudo- second -order model	Elovich	Bangham
Mg-Al-CO_3	0.961	0.864	0.995	0.99	0.972
Mg-Al-400	0.929	0.935	0.987	0.976	0.988
Mg-Al-500	0.885	0.976	0.984	0.975	0.998
Mg-Al-600	0.857	0.977	0.97	0.958	0.998
Mg-Al-700	0.801	0.971	0.974	0.928	0.996

4 Conclusion

The characteristics, mechanism and adsorption kinetics of removing HCl by Mg-Al-CO_3 and calcined Mg-Al adsorbents were investigated.

According to the results of ICP-OES, XRD, and SEM, the layered structure of Mg-Al-CO_3 with a molar ratio of Mg/Al =3.1 was successfully prepared by the coprecipitation method. TGA analysis showed that Mg-Al-CO_3 had three weight loss stages, with the highest weight loss observed in stage II, reaching 26.8 %.

The breakthrough chlorine capacity of Mg-Al-CO_3 decreased as the temperature increased

from 300 to 700 °C. The optimal performance in removing HCl of Mg-Al-CO_3 was observed at 300 °C with a breakthrough chlorine capacity of 102.7 mg/g. The performance of removing HCl by calcined Mg-Al adsorbents at 300 °C decreased as the calcined temperature increased from 400 to 700 °C. Among them, Mg-Al-400 showed the better performance in HCl removal, with an average HCl removal rate of 90.11% within the first 120 min, and a breakthrough chlorine capacity of 120.1 mg g^{-1}. The HCl removal performance of Mg-Al-400 decreased with the increasing flow rate. Specifically, when the flow rate increased from 0.5 to 2 L/min, the average HCl removal rate decreased from 90.11% to 45.16%, the breakthrough chloride capacity decreased from 120.1 to 29.7 mg g^{-1}.

In terms of reaction mechanism, both physical and chemical reactions occurred during the process of HCl adsorption, with the chemical reaction being the main controlling one. There are two reaction paths for Mg-Al-400, the first involves the reaction of Mg with Cl^- to generate $MgCl_2$, while the second involves Cl^- acting as a new interlayer anion of hydrotalcite. According to the results of adsorption kinetics, both the pseudo-second-order and the Bangham model fitted well with the HCl removal process of Mg-Al-400.

Credit author statement

Songshan Cao: Methodology, experiments, data curation, writing-original draft. Jun Cao: Review & editing. Hualun Zhu: Review & editing. Yaji Huang: Supervision. Baosheng Jin: Supervision. Massimiliano Materazzi: Review & supervision.

Acknowledgements

This work was supported by National Natural Science Foundation of China (52076067), the Natural Science Foundation of Jiangsu Province (BK20201319), Carbon Peak and Carbon Neutrality Science Technology Innovation Special Funds (Major Scientific and Technological Achievements Transformation) Project of Jiangsu Province (SBA2022080063), and the Postgraduate Research & Practice Innovation Program of Jiangsu Province (KYCX20_0097).

Reference:

[1] Wang F, Harindintwali JD, Yuan Z, Wang M, Wang F, Li S, et al. Technologies and perspectives for achieving carbon neutrality. The Innovation 2021;2(4):100180.

[2] Maximillian J, Brusseau M, Glenn E, Matthias A. Pollution and environmental perturbations in the global system. Environmental and pollution science. Elsevier; 2019, p. 457-76.

[3] Qiu Y, Ma L, Zeng D, Li M, Cui D, Lv Y, et al. Efficient CO_2 to CO conversion at moderate temperatures enabled by the cobalt and copper co-doped ferrite oxygen carrier. Journal of Energy Chemistry 2020;46:123-32.

[4] Chen L, Msigwa G, Yang M, Osman AI, Fawzy S, Rooney DW, et al. Strategies to achieve a carbon neutral society: a review. Environmental Chemistry Letters 2022.

[5] Díaz-Pérez MA, Serrano-Ruiz JC. Catalytic Production of Jet Fuels from Biomass. Molecules 2020;25(4):802.

[6] Chen T, Cao J, Jin B. Oxygen-Enriched Gasification of Dried Sewage Sludge, Refuse-Derived Fuel, and Their Cogasification in a Laboratory-Scale Fluidized Bed. Industrial & Engineering Chemistry Research 2018;58(1):479-86.

[7] Zhu H, Chen Z, Pastor-Perez L, Long X, Millan M. How syngas composition affects catalytic steam reforming of tars: An analysis using toluene as model compound. International Journal of Hydrogen Energy 2023;48(4):1290-303.

[8] Cao S, Duan F, Wang P, Chyang C. Biochar contribution in biomass reburning technology and transformation mechanism of its nitrogen foundational groups at different oxygen contents. Energy 2018;155:272-80.

[9] He D, Hu H, Jiao F, Zuo W, Liu C, Xie H, et al. Thermal separation of heavy metals from municipal solid waste incineration fly ash: A review. Chemical Engineering Journal 2023:143344.

[10] Sahu TK, Sahu VK, Mondal A, Shukla PC, Gupta S, Sarkar S. Investigation of sugar extraction capability from rice paddy straw for potential use of bioethanol production towards energy security. Energy Sources, Part A: Recovery, Utilization, and Environmental Effects 2022;44(1):272-86.

[11] Chen T, Cao J, Jin B. The effect of rice straw gasification temperature on the release and occurrence modes of Na and K in a fluidized bed. Applied Sciences 2017;7(12):1207.

[12] Radha S, Navrotsky A. Energetics of CO_2 Adsorption on Mg–Al Layered Double Hydroxides and Related Mixed Metal Oxides. The Journal of Physical Chemistry C 2014;118(51):29836-44.

[13] Paramita W, Hartono DM, Soesilo TEB. Sustainability of Refuse Derived Fuel Potential from Municipal Solid Waste for Cement's Alternative Fuel in Indonesia (A Case at Jeruklegi Landfill, in Cilacap). IOP Conference Series: Earth and Environmental Science 2018;159:012027.

[14] Beckmann M, Pohl M, Pieper C, Bohme R, Bernhardt D, Bohning D, et al. Usage of Alternative Fuels in Power Plants. CHEMIE INGENIEUR TECHNIK 2011;83(11):1864-79.

[15] Zhu HL, Papurello D, Gandiglio M, Lanzini A, Akpinar I, Shearing PR, et al. Study of H2S removal capability from simulated biogas by using waste-derived adsorbent materials. Processes 2020;8(9):1030.

[16] Ren X, Meng X, Panahi A, Rokni E, Sun R, Levendis YA. Hydrogen chloride release from combustion of Corn Straw in a fixed bed. Journal of Energy Resources Technology 2018;140(5).

[17] Wang B, Gao X, Huang J, Mofrad AZ, Wang Z, Feng C, et al. Transformation of HCl during pyrolysis of biomass and its model compounds. Fuel 2022;309:122139.

[18] Marcantonio V, Müller M, Bocci E. A Review of Hot Gas Cleaning Techniques for Hydrogen Chloride Removal from Biomass-Derived Syngas. Energies 2021;14(20):6519.

[19] Ephraim A, Ngo L, Pham Minh D, Lebonnois D, Peregrina C, Sharrock P, et al. Valorization of Waste-Derived Inorganic Sorbents for the Removal of HCl in Syngas. Waste and Biomass Valorization 2019;10(11):3435-46.

[20] Bal M, Siddiqi H, Mukherjee S, Meikap B. Design of self priming venturi scrubber for the simultaneous abatement of HCl gas and particulate matter from the flue gas. Chemical Engineering Research and Design 2019;150:311-9.

[21] Ding X, Yang Y, Zeng Z, Huang Z. Insight into the Transformation Behaviors of Dioxins from Sintering Flue Gas in the Cyclic Thermal Regeneration by the V_2O_5/AC Catalyst-sorbent. Environmental Science & Technology 2022;56(9):5786-95.

[22] Ding X, Chang K, Tian J, Yang Y, Jiao W, Hou Y, et al. Effects of pore structures and multiple components in flue gas on the adsorption behaviors of dioxins by activated carbon. Colloids and Surfaces A: Physicochemical and Engineering Aspects 2023;661:130868.

[23] Ngoc Lan Thao NT, Chiang K-Y, Wan H-P, Hung W-C, Liu C-F. Enhanced trace pollutants removal efficiency and hydrogen production in rice straw gasification using hot gas cleaning system. International Journal of Hydrogen Energy 2019;44(6):3363-72.

[24] Kim K-D, Jeon S-M, Hasolli N, Lee K-S, Lee J-R, Han J-W, et al. HCl removal characteristics of calcium hydroxide at the dry-type sorbent reaction accelerator using municipal waste incinerator flue gas at a real site. Korean Journal of Chemical Engineering 2017;34(3):747-56.

[25] Ren X, Rokni E, Liu Y, Levendis YA. Reduction of HCl emissions from combustion of biomass by alkali carbonate sorbents or by thermal pretreatment. Journal of Energy Engineering 2018;144(4):04018045.

[26] Dal Pozzo A, Lazazzara L, Antonioni G, Cozzani V. Techno-economic performance of HCl and SO2 removal in waste-to-energy plants by furnace direct sorbent injection. Journal of Hazardous Materials 2020;394:122518.

[27] Dal Pozzo A, Guglielmi D, Antonioni G, Tugnoli A. Environmental and economic performance assessment of alternative acid gas removal technologies for waste-to-energy plants. Sustainable Production and Consumption 2018;16:202-15.

[28] Cao J, Zhong W, Jin B, Wang Z, Wang K. Treatment of hydrochloric acid in flue gas from municipal solid waste incineration with Ca–Mg–Al mixed oxides at medium–high temperatures. Energy & fuels 2014;28(6):4112-7.

[29] Kameda T, Takahashi Y, Kumagai S, Saito Y, Fujita S, Itou I, et al. Exhaust gas treatment using MnO2/Mg–Al layered double hydroxide: Assessment of its mixed gas removal performance and regeneration. Chemical Engineering Research and Design 2022;178:602-8.

[30] Veksha A, Giannis A, Oh W-D, Chang VWC, Lisak G. Upgrading of non-condensable pyrolysis gas from mixed plastics through catalytic decomposition and dechlorination. Fuel

Processing Technology 2018;170:13-20.

[31] Liang S, Fan Z, Zhang W, Guo M, Cheng F, Zhang M. Inexpensive metal oxides nanoparticles doped Na2CO3 fibers for highly selective capturing trace HCl from HCl/CO_2 mixture gas at low temperature. Chemical Engineering Journal 2018;352:634-43.

[32] Liu G, Wang H, Deplazes S, Veksha A, Wirz-Töndury C, Giannis A, et al. Ba–Al-decorated iron ore as bifunctional oxygen carrier and HCl sorbent for chemical looping combustion of syngas. Combustion and Flame 2021;223:230-42.

[33] Pachitsas S, Wedel S, Jensen LS, Illerup JB, Dam-Johansen K. Experimental evaluation of hydrogen chloride (HCl) absorption by cement raw meals at low temperatures, using fixed-bed tests. Journal of Environmental Chemical Engineering 2019;7(2):102959.

[34] Faramawy S, Zaki T, Sakr AAE, Saber O, Aboul-Gheit AK, Hassan SA. The activity of Mg-Al layered double hydroxides intercalated with nitrogen-containing anions towards the removal of carbon dioxide from natural gas. Journal of Natural Gas Science and Engineering 2018;54:72-82.

[35] Cao J, Chen T, Jin B, Huang Y, Hu C. Structural Effects of HCl Adsorption on Mg–Fe Hydrotalcite-like Oxides at 350–650 °C in Flue Gas. Industrial & Engineering Chemistry Research 2018;57(44):14939-47.

[36] Cao J, Chen T, Jin B, Huang Y, Hu C. Adsorption of HCl on calcined Ca and Zn hydrotalcite-like compounds (HTLs) at medium-high temperature in flue gas. Industrial & Engineering Chemistry Research 2018;58(1):18-26.

[37] Julianti NK, Wardani TK, Gunardi I, Roesyadi A. Effect of calcination at synthesis of Mg-Al hydrotalcite using co-precipitation method. The Journal of Pure and Applied Chemistry Research 2017;6(1):7.

[38] El Gaini L, Lakraimi M, Sebbar E, Meghea A, Bakasse M. Removal of indigo carmine dye from water to Mg–Al–CO_3-calcined layered double hydroxides. Journal of Hazardous Materials 2009;161(2-3):627-32.

[39] Wan D, Liu Y, Xiao S, Chen J, Zhang J. Uptake fluoride from water by caclined Mg-Al-CO3 hydrotalcite: Mg/Al ratio effect on its structure, electrical affinity and adsorptive property. Colloids and Surfaces A: Physicochemical and Engineering Aspects 2015;469:307-14.

[40] Kim Y, Yang W, Liu PK, Sahimi M, Tsotsis TT. Thermal evolution of the structure of a Mg− Al− CO3 layered double hydroxide: sorption reversibility aspects. Industrial & engineering chemistry research 2004;43(16):4559-70.

[41] Phuong T, Cong TD, Ta VT, Nguyen TH. Study on Leaching of Phosphate from Municipal Wastewater Treatment Plant's Sewage Sludge and Followed by Adsorption on Mg-Al Layered Double Hydroxide. Journal of Nanomaterials 2022;2022:1777187.

[42] Ni Z, Chen A, Fang C, Wang L, Yu W. Enhanced NOx adsorption using calcined Zn/Mg/Ni/Al hydrotalcite-like compounds. Journal of Physics and Chemistry of Solids 2009;70(3):632-8.

[43] Zhao L, Li X, Hao C, Raston CL. SO_2 adsorption and transformation on calcined NiAl hydrotalcite-like compounds surfaces: An in situ FTIR and DFT study. Applied Catalysis B: Environmental 2012;117-118:339-45.

[44] Ji C, Wang Y, Zhao N. Synthesis of CuAl hydrotalcite-SBA-15 composites and CO_2 capture using the sorbent. Applied Surface Science 2019;481:337-43.

[45] Kameda T, Tochinai M, Kumagai S, Yoshioka T. Treatment of HCl gas by cyclic use of Mg–Al layered double hydroxide intercalated with CO_3^{2-}. Atmospheric Pollution Research 2020;11(2):290-5.

[46] Kameda T, Takahashi Y, Kumagai S, Saito Y, Fujita S, Itou I, et al. Comparison of Mg–Al layered double hydroxides intercalated with OH^- and CO_3^{2-} for the removal of HCl, SO_2, and NO2. Journal of Porous Materials 2022;29(3):723-8.

[47] Zhang L, Cao S, Li Z, Zhang H, Duan F. Pore structure of sludge char and simultaneously NO removal characteristics in the treated flue gas from Ca-L. Fuel 2021;289:119937.

[48] Mane VS, Mall ID, Srivastava VC. Kinetic and equilibrium isotherm studies for the adsorptive removal of Brilliant Green dye from aqueous solution by rice husk ash. Journal of environmental management 2007;84(4):390-400.

[49] Hubbe MA, Azizian S, Douven S. Implications of apparent pseudo-second-order adsorption kinetics onto cellulosic materials: A review. BioResources 2019;14(3).

[50] Aharoni C, Sideman S, Hoffer E. Adsorption of phosphate ions by collodion-coated alumina. Journal of Chemical Technology and Biotechnology 1979;29(7):404-12.

[51] Ziyat H, Naciri Bennani M, Hajjaj H, Mekdad S, Qabaqous O. Synthesis and characterization of crude hydrotalcite Mg–Al–CO3: study of thymol adsorption. Research on Chemical Intermediates 2018;44(7):4163-77.

[52] Phuong T, Cong TD, Ta VT, Nguyen TH. Study on Leaching of Phosphate from Municipal Wastewater Treatment Plant's Sewage Sludge and Followed by Adsorption on Mg-Al Layered Double Hydroxide. Journal of Nanomaterials 2022;2022:1-9.

[53] Baek J-I, Eom TH, Lee JB, Jegarl S, Ryu CK, Park YC, et al. Cleaning of gaseous hydrogen chloride in a syngas by spray-dried potassium-based solid sorbents. Korean Journal of Chemical Engineering 2015;32:845-51.

[54] Mahamud MM, Novo MF. The use of fractal analysis in the textural characterization of coals. Fuel 2008;87(2):222-31.

[55] Tan K, Hameed B. Insight into the adsorption kinetics models for the removal of contaminants from aqueous solutions. Journal of the Taiwan Institute of Chemical Engineers 2017;74:25-48.